Boosting tenfold recycling profit by a one-step calcination strategy for upcycling spent $LiCoO_2$ to high-value Li_6CoO_4

Xingguo Zhong[1,3†], Peipei Du[2†], Ziwen Yang[1], Gaofeng Du[1], Xinqi Wei[1], Haoyue Liang[1], Xuhao Liu[1], Yalun Li[3], Wei Liang[3], Jinxing Huang[3], Yanpeng Guo[1], Xizheng Liu[2], Tianyou Zhai[1*]and Huiqiao Li[1*]

[1]State Key Laboratory of Materials Processing and Die & Mould Technology, School of Materials Science and Engineering, Huazhong University of Science and Technology, Wuhan, P. R. China.

[2]Key Laboratory of Flexible Optoelectronic Materials and Technology, Ministry of Education, School of Optoelectronic Materials and Technology, Jianghan University, Wuhan, P. R. China.

[3]Cornex New Energy Limited, Yichang, P. R. China.

* To whom correspondence should be addressed: hqli@hust.edu.cn

Methods

Materials and regeneration process

The collected waste LCO batteries are processed through discharging, disassembling, and separation to obtain spent LCO cathode electrode, followed by atmospheric calcination at 450℃ for 2 hours to eliminate residual carbon and PVDF additives. C- Li_6CoO_4 was synthesized via a two-stage sintering: the spent LCO and carbon (Super P) were mixed and heated to 550℃ for 4 hours at a heating rate of 5°C/min, followed by secondary sintering of the intermediate products with lithium sources to 650°C for 8 hours. R-Li_6CoO_4 was synthesized through ball-milling of glucose and s-LCO in a zirconia jar at 400 rpm, then the mixture with 5% additional Li_2O (the Li/Co molar ratio is 6.05:1) was sintered at 550°C for 2 hours and 650°C for 8 hours with a heating rate of 5°C/min in an argon atmosphere. Finally, the aforementioned materials naturally cooled down. LFP, graphite, Li_5FeO_5, and Li_2NiO_2 were procured directly from Canrd New Energy official platform without further modification.

Battery assembly and electrochemical test

When evaluating the performance of Li_6CoO_4, the electrode was prepared using Li_6CoO_4, Super P, and PVDF binder with a weight ratio of 80:10:10; Other cathode electrodes (LFP, and 5% Li_6CoO_4+LFP) were mixed by active material, Super P, and PVDF binder with a weight ratio of 90:5:5, while N-methyl-2 pyrrolidone (NMP) with ~2 times of the total mass was added to prepare a homogeneous slurry. They were coated onto aluminum foil and vacuum-dried (90°C/12h), achieving active material loadings of 5.0 $mg \cdot cm^{-2}$. Graphite anodes were similarly processed using aqueous slurry (Gr: Super P: SBR: CMC=90:4:2:4 wt%) on copper foil and vacuum-dried (80°C/12h) with 2.5 $mg \cdot cm^{-2}$ loading. CR2032 coin cells were assembled in an Ar glovebox with 60 μL L1376 electrolyte (Canrd New Energy). Electrochemical testing was performed using a Neware system for rate capability (0.1-5C, 1C=150 $mA \cdot g^{-1}$) and cycling stability evaluation. EIS were derived from a CHI660e workstation (0.1 Hz-1000kHz, 10 mV

amplitude) for charge transfer resistance analysis.

Characterization methods

The temperature-dependent in-situ XRD measurements were conducted on the Bruker D8 instrument, and the other XRD patterns were conducted using the Bruker D2 instrument (Bruker AXS D2 Advance with Cu-Kα radiation, λ=1.54178Å). The SEM images and EDX mappings were collected on a Quanta650 FEG instrument. The TEM investigations were conducted using the Tecnai G2 high-resolution instrument. The XPS data were measured by a monochromatic Al-Kα X-ray source using a SHIMADZU AXIS SUPRA$^+$.

Universality of this upcycling strategy

In addition to the s-LCO mentioned in the main text, we also successfully reconstructed LCO samples with different health conditions into Li_6CoO_4 using the same method. The spent LCO sample possessed a residual capacity of 40%, and the lithium-to-cobalt atomic ratio is 0.538 (Supplementary Fig. 18a and b). As shown in Supplementary Fig. 18a and b. As usage increases, the damage to the crystal structure becomes more severe, and the content of Co_3O_4 also rises accordingly. When the weight ratio of glucose: Li_2O: LCO is 0.15:1.7:1, the Li_6CoO_4 phase appeared. The delithiation capacity of the obtained Li_6CoO_4 is consistent with R-Li_6CoO_4, which is as high as 856.8 mAh g^{-1} (supplementary Fig. 19). These results indicate that the capacity performance of recycled products (Li_6CoO_4) is independent of the health status and Li content of s-LCO precursor, making the recycling technology universal.

Supplementary Figures

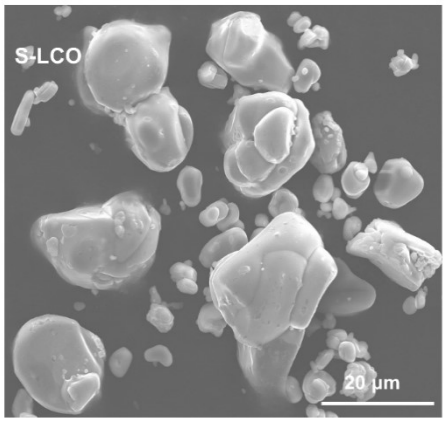

Supplementary Fig. 1| SEM image of the s-LCO sample.

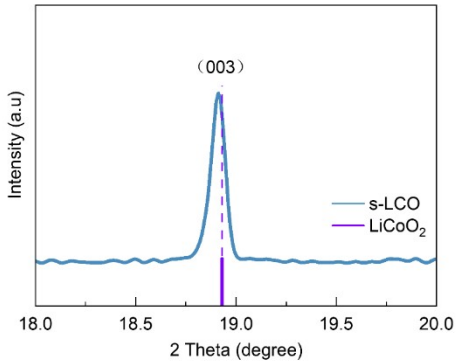

Supplementary Fig. 2| The (003) peak extracted from the XRD pattern of the s-LCO sample.

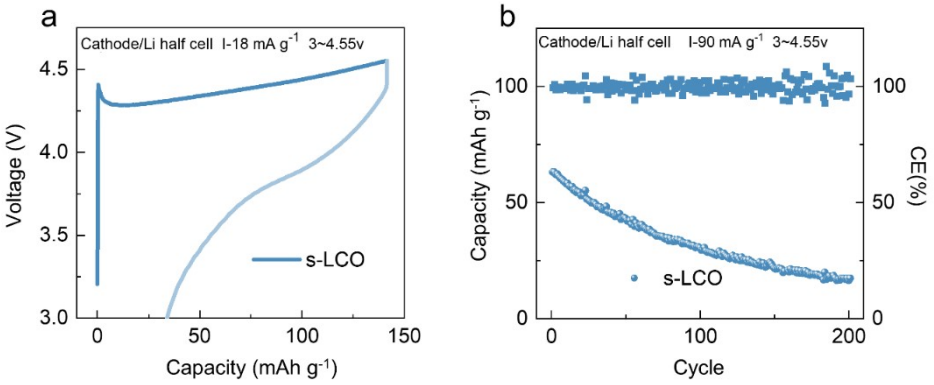

Supplementary Fig. 3| The charge-discharge curve (a) and long-term cycling capacity retention (b) of s-LCO.

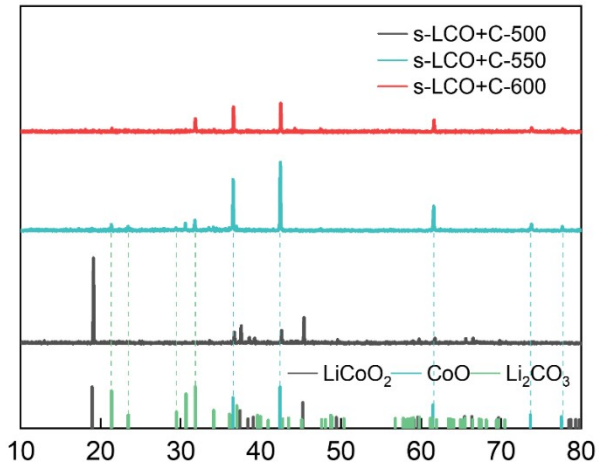

Supplementary Fig. 4| XRD patterns of the reaction products of s-LCO and carbon at different temperatures.

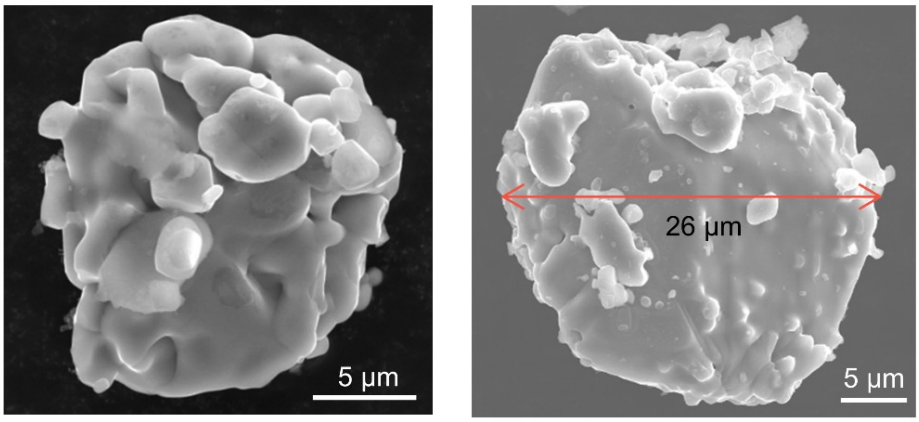

Supplementary Fig. 5| SEM images of the reaction products of the s-LCO and carbon at 550 ℃.

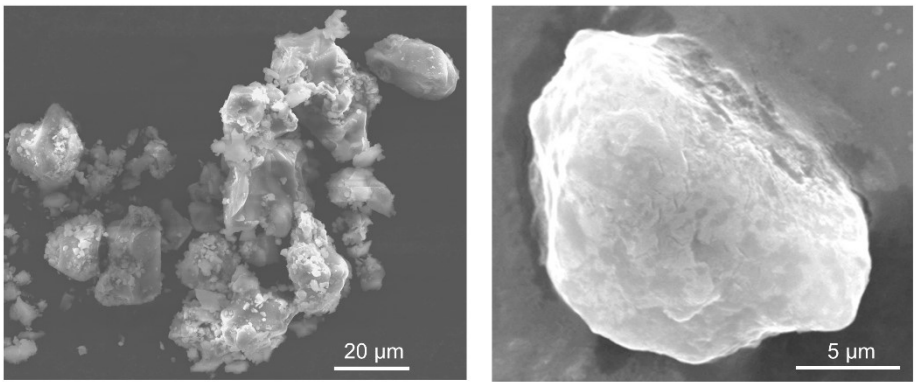

Supplementary Fig. 6| SEM images of the C-Li_6CoO_4 sample.

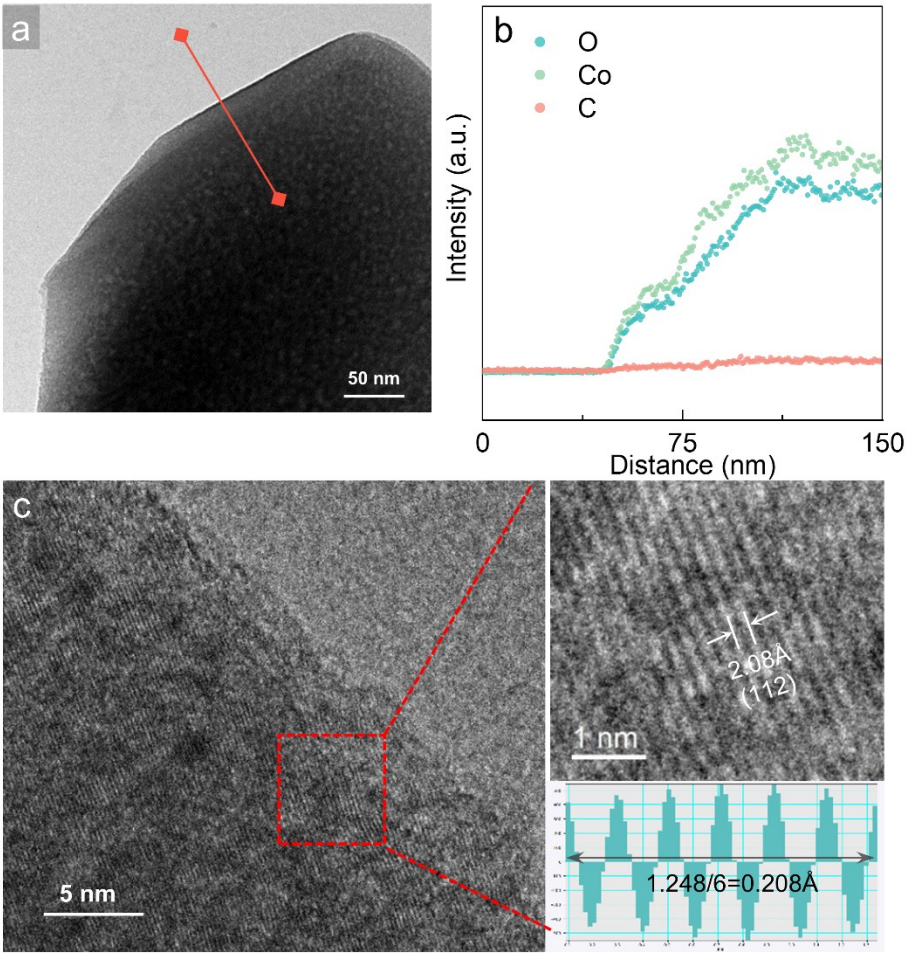

Supplementary Fig. 7| (a) TEM image of C-Li_6CoO_4 sample. (b) The EDS line-scan spectra from the partical surface to the bulk. (c) HRTEM image of the C-Li_6CoO_4.

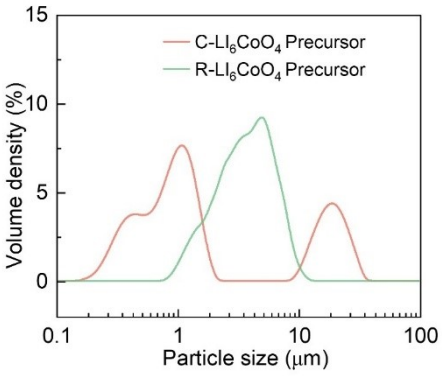

Supplementary Fig. 8| Particle size plots of C-Li_6CoO_4 and R-Li_6CoO_4 precursors, where the C-Li_6CoO_4 precursor refers to the reaction products of s-LCO and carbon at 550°C and the R-Li6CoO4 precursor refers to the mixture of s-LCO, glucose and Li_2O after milling.

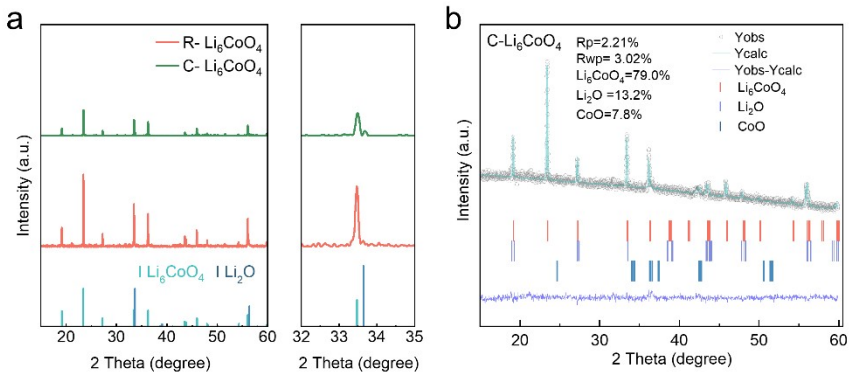

Supplementary Fig. 9| (a) Comparison of XRD patterns for C-Li_6CoO_4 and R-Li_6CoO_4. (b) The Rietveld refinements of XRD for C-Li_6CoO_4.

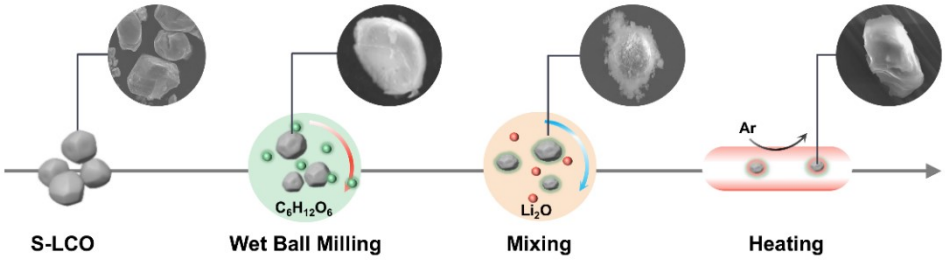

Supplementary Fig. 10| The recycling process from s-LCO to R-Li_6CoO_4.

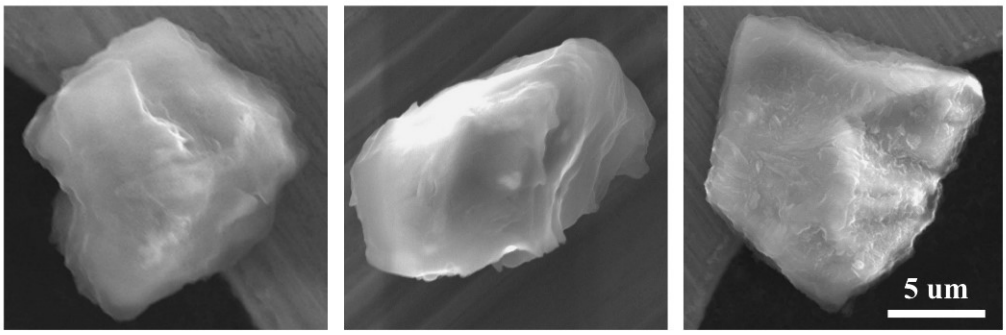

Supplementary Fig. 11| SEM images of R-Li_6CoO_4.

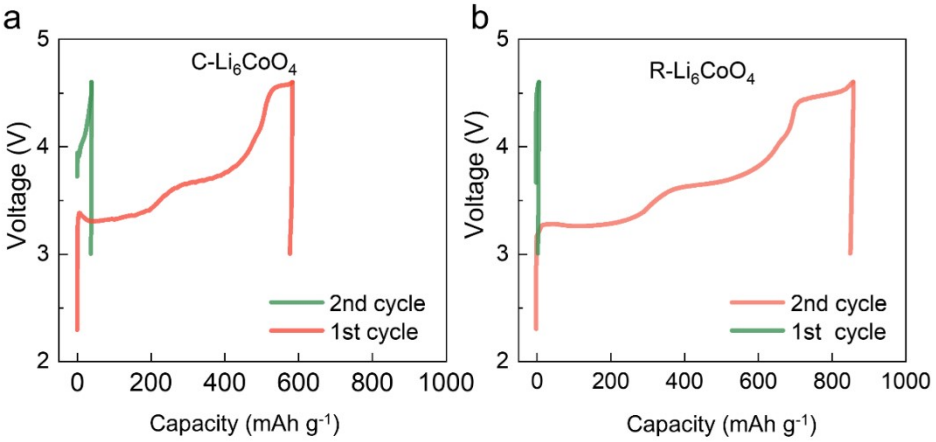

Supplementary Fig. 12| The first two cycles of charge-discharge curves for C-Li_6CoO_4 (a) and R-Li_6CoO_4 (b).

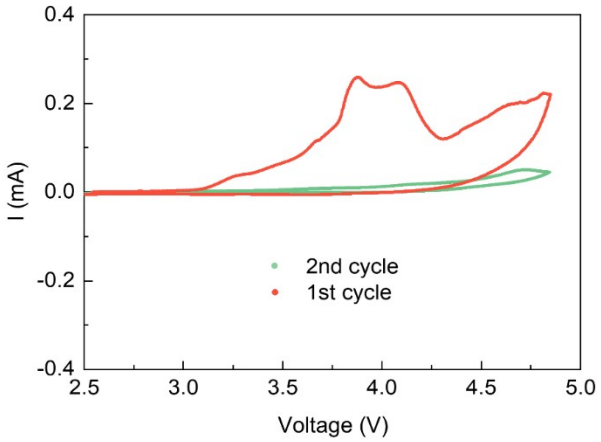

Supplementary Fig. 13| CV curves of the first two cycles for R-Li_6CoO_4 at 0.1 mV s^{-1}.

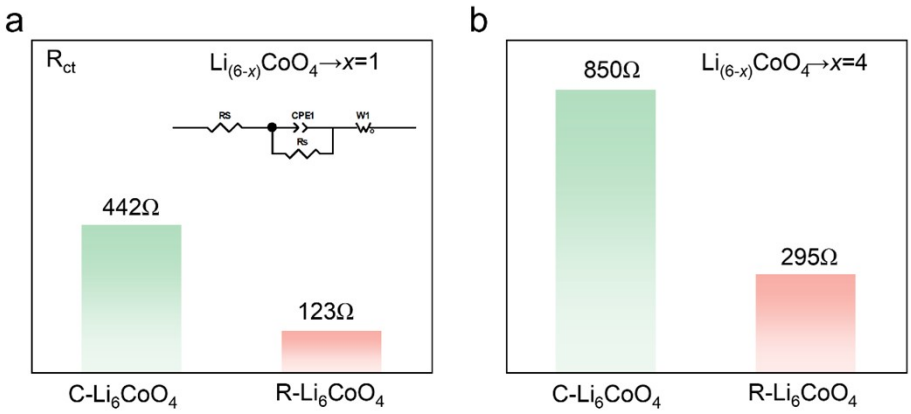

Supplementary Fig. 14| R_{ct} of C-Li_6CoO_4 and R-Li_6CoO_4 When it is delithiated to x=1 (a) and x=4 (b).

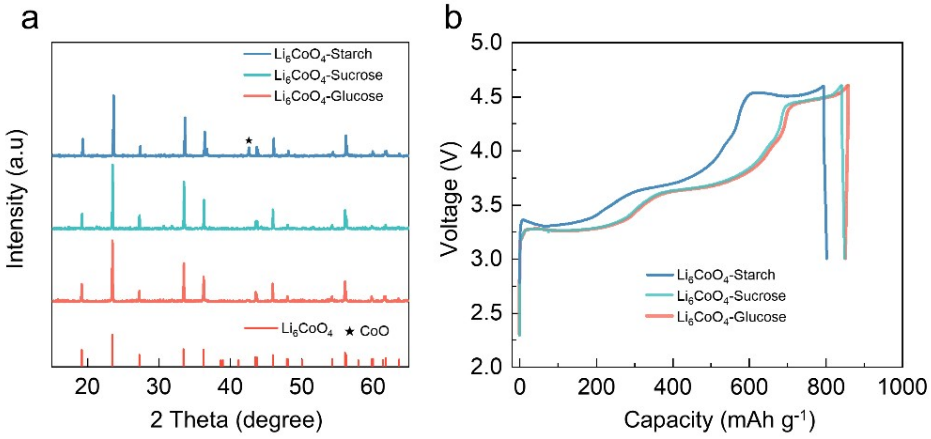

Supplementary Fig. 15| (a) XRD patterns of the synthesized products with different sugars. (b)The first-cycle charge-discharge curves of the synthesized products with different sugars.

When using sucrose as the precursor, the purity and delithiation capacity of the synthesized Li_6CoO_4 are similar to those obtained using glucose. When using starch as the reactant, the synthesized products contained a small amount of unreacted CoO except for Li_6CoO_4. The possible reason may be that the poor thermal stability of starch results in a carbon layer with a low degree of graphitization after carbonization. This leads to inferior electrical conductivity compared to sucrose and glucose, causing significant voltage polarization during lithium deintercalation in Li_6CoO_4 and consequently lower deintercalation capacity.

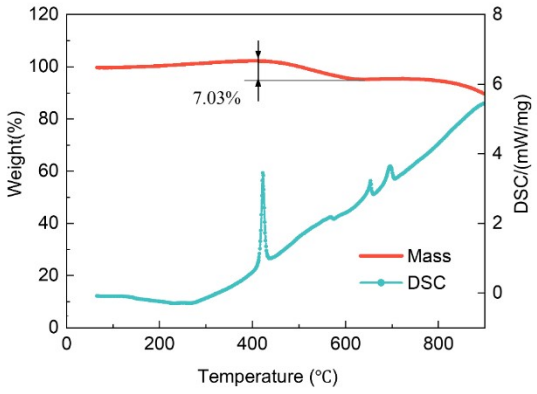

Supplementary Fig. 16| TG-DSC curves of the s-LCO, glucose, and Li_2O mixtures.

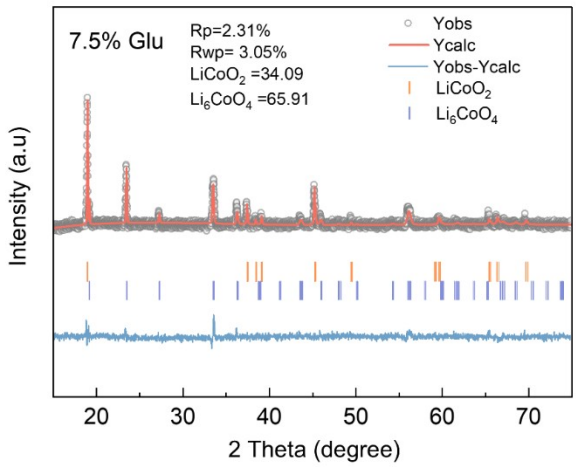

Supplementary Fig. 17| Rietveld refinement profiles with the glucose content of 7.5%.

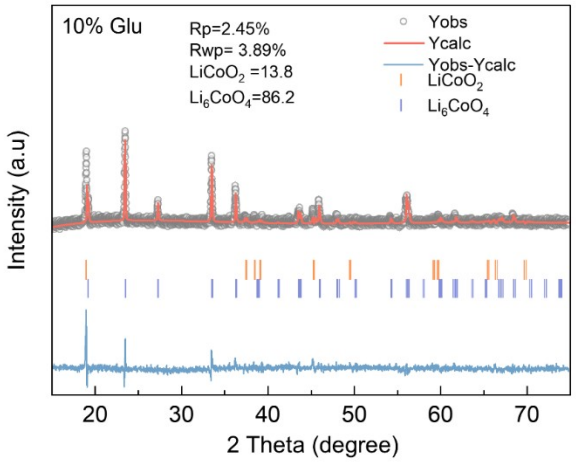

Supplementary Fig. 18| Rietveld refinement profiles with the glucose content of 10%.

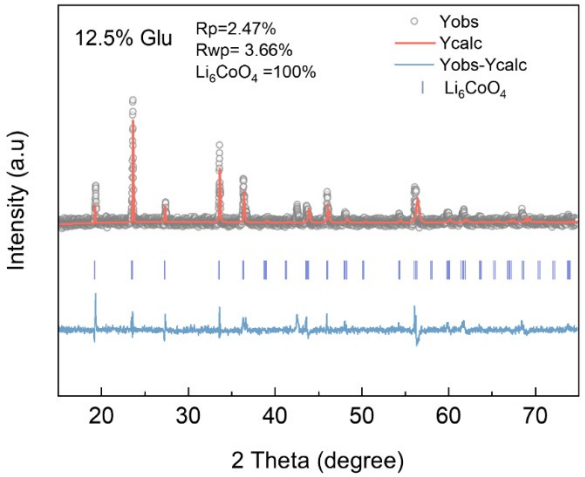

Supplementary Fig. 19| Rietveld refinement profile with the glucose content of 12.5%.

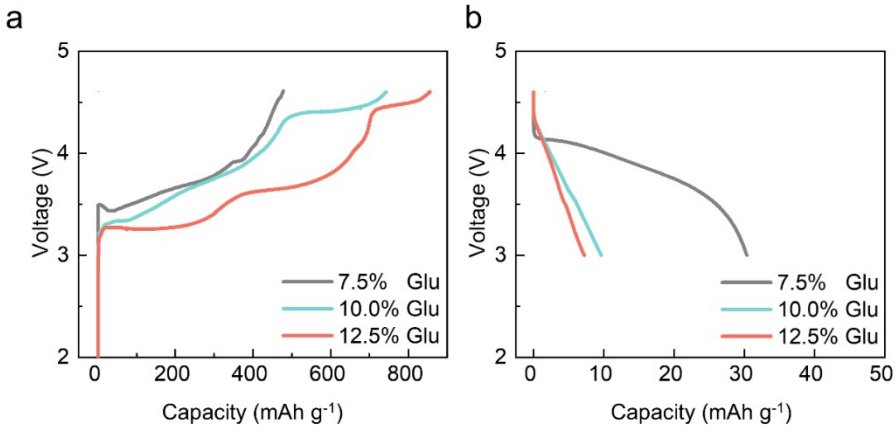

Supplementary Fig. 20| Charge-discharge curves of the samples with different glucose concentrations.

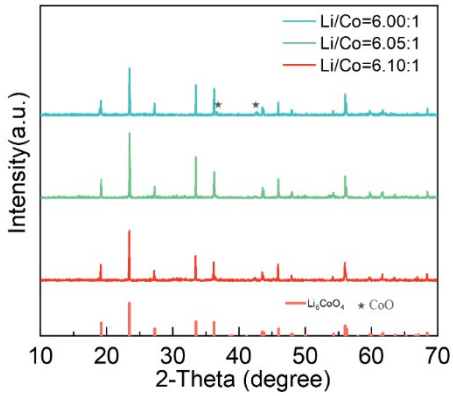

Supplementary Fig. 21| Comparison of XRD patterns of R-Li_6CoO_4 with different Li/Co molar ratio.

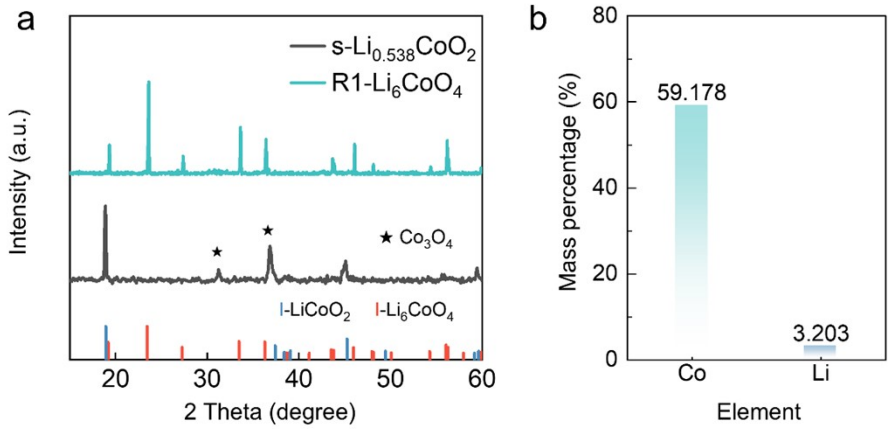

Supplementary Fig. 22| (a) XRD patterns of s-$Li_{0.538}CoO_2$ and R1-Li_6CoO_4. (b) ICP results of s-$Li_{0.538}CoO_2$.

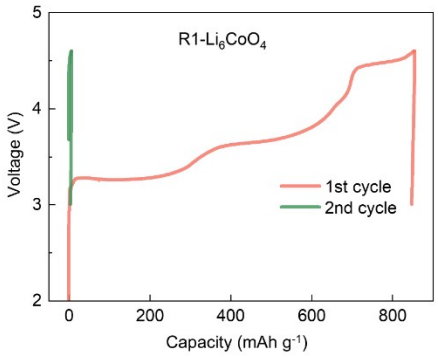

Supplementary Fig. 23| The first two cycles of charge-discharge curves for R1-Li_6CoO_4.

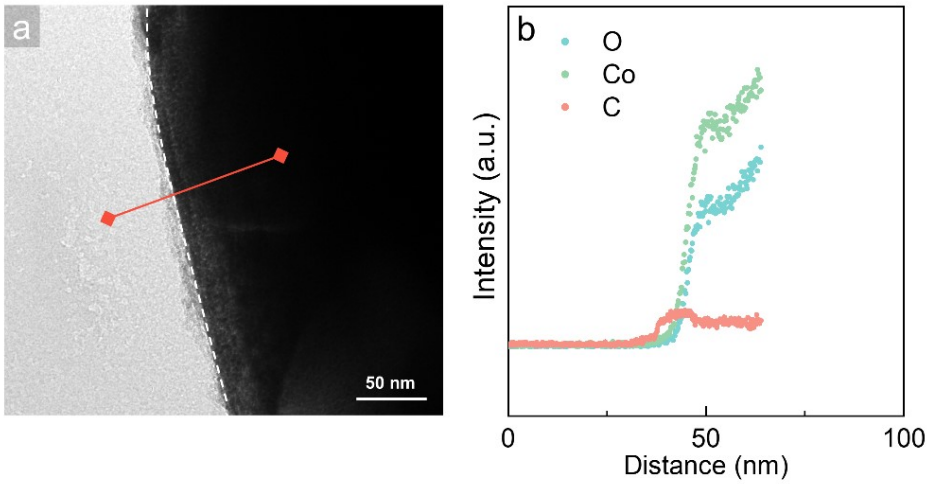

Supplementary Fig. 24| (a) TEM image of R-Li_6CoO_4 sample. (b) The EDS line-scan spectra from the partical surface to the bulk.

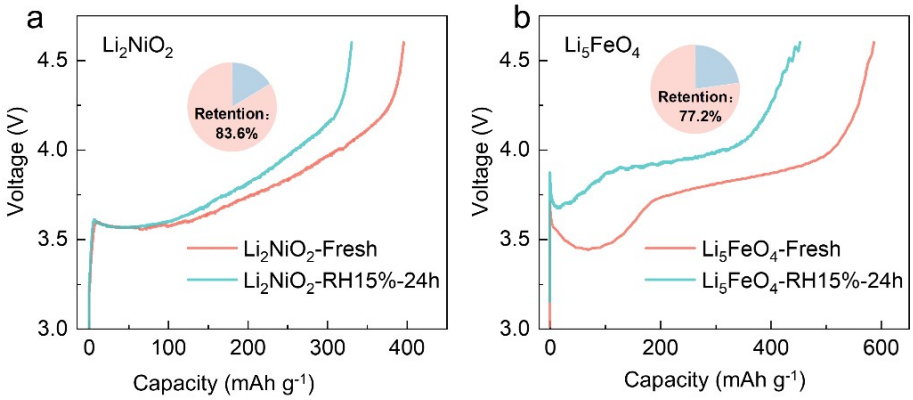

Supplementary Fig. 25| The first charge curves of LNO (a) and LFO (b) before and after exposure in the atmosphere with the 15% humidity for 24 hours.

Supplementary Fig. 26| The first charge curve of C- Li_6CoO_4 exposure for 24 hours in the air with a humidity of 15%.

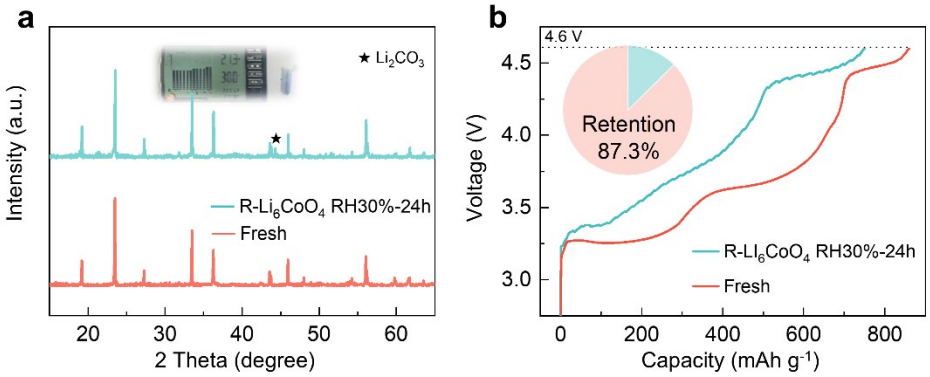

Supplementary Fig. 27| (a) XRD patterns before and after atmospheric exposure with 30% humidity. (b) Comparison of the first charge curves before and after exposure in the atmosphere with the 30% humidity for 24 hours.

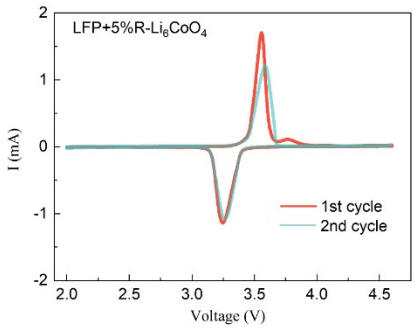

Supplementary Fig. 28| CV curves of the first two cycles for LFP+5%R-Li_6CoO_4 cathode at 0.1 mV s^{-1}.

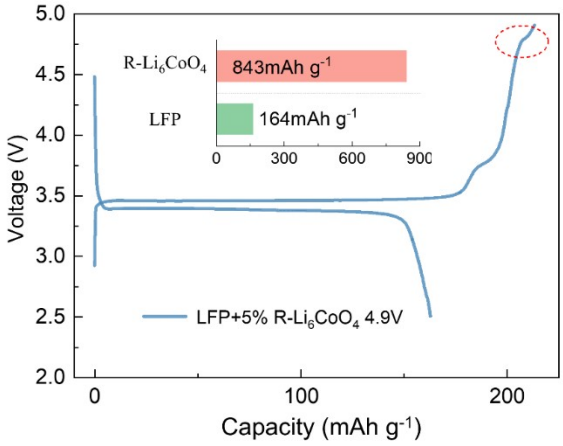

Supplementary Fig. 29| The first charge-discharge curve of LFP with 5% R-Li_6CoO_4 when charged to 4.9 V.

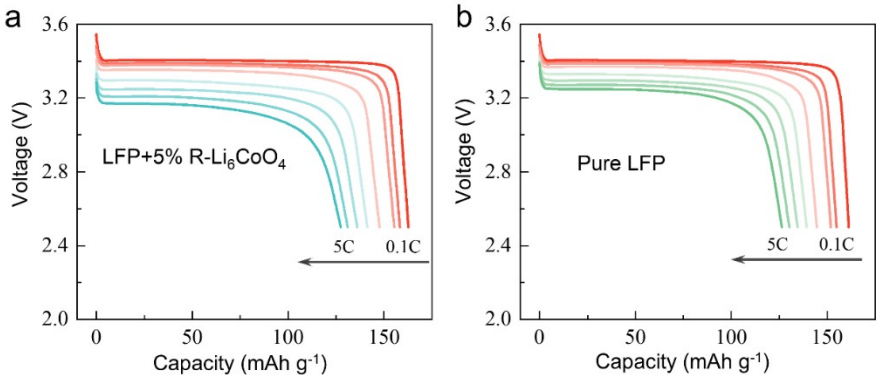

Supplementary Fig. 30| The discharge curves measured at various rates of LFP+5%R-Li_6CoO_4 (a) and Pure LFP (b).

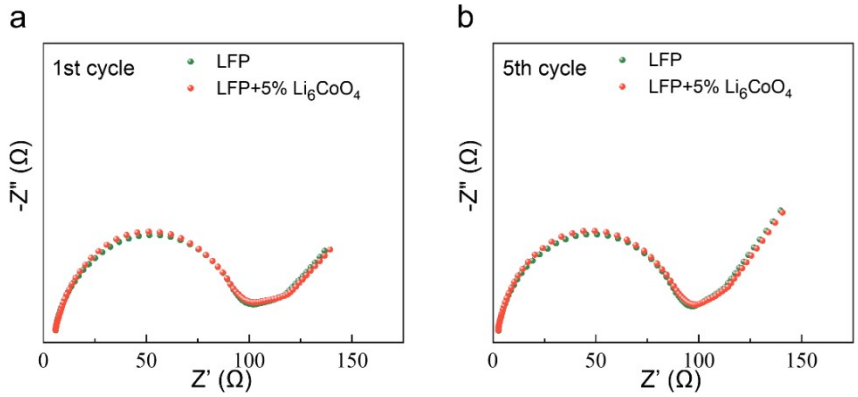

Supplementary Fig. 31| EIS Comparison of LFP and LFP+5% Li_6CoO_4 in the first and fifth cycles.

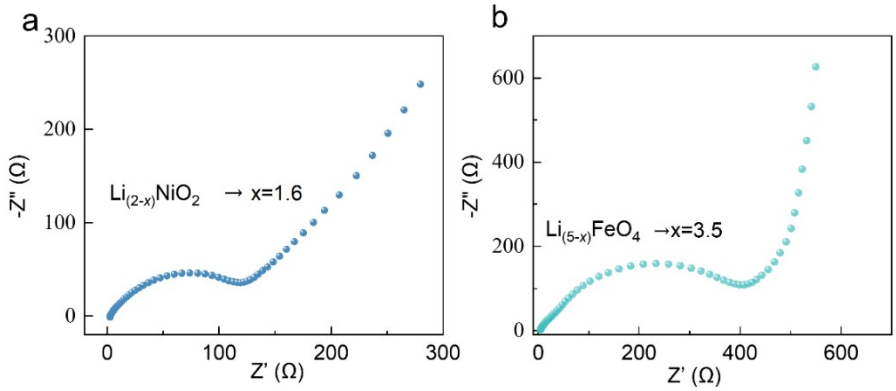

Supplementary Fig. 32| EIS analysis of Li_2NiO_2 (a) and Li_5FeO_4 (b) at different delithiation capacities.

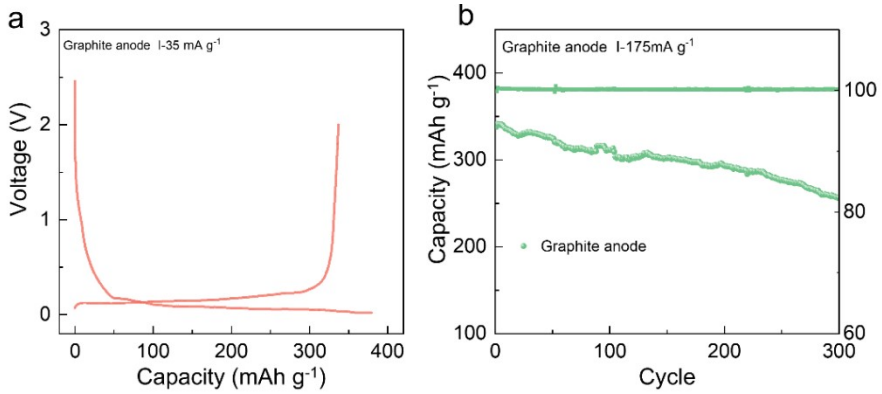

Supplementary Fig. 33| The charge-discharge curve at 0.1C (a), long-term cycling stability (b), and CE of 0.5C for graphite anode.

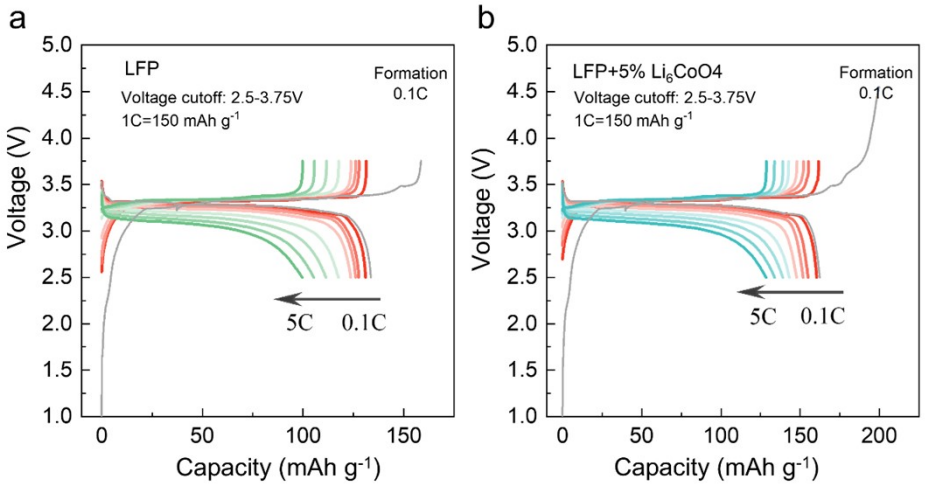

Supplementary Fig. 34| The charge-discharge curves of LFP/Gr full cell (a) and LFP+5%R-Li_6CoO_4/Gr full cell (b) measured at various rates.

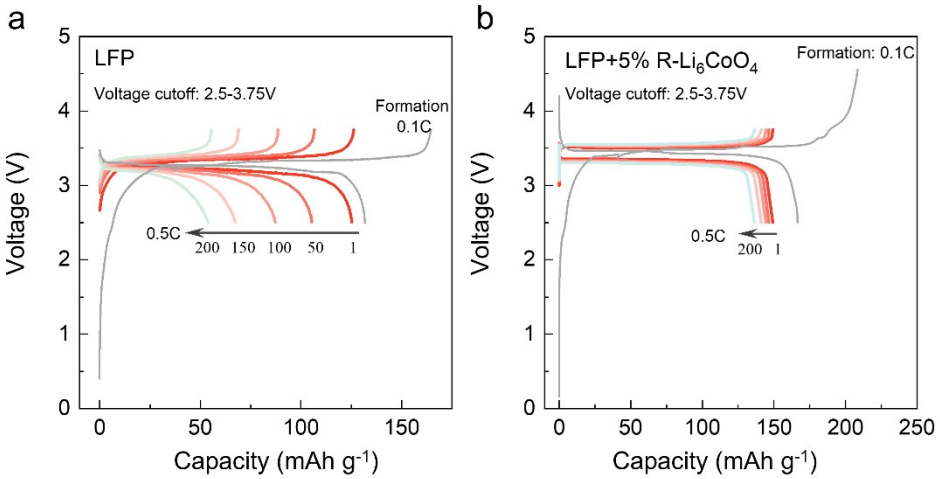

Supplementary Fig. 35| The discharge curves of different cycles at 0.5C for LFP/Gr full cell (a) and LFP+5%R-Li_6CoO_4/Gr full cell (b).

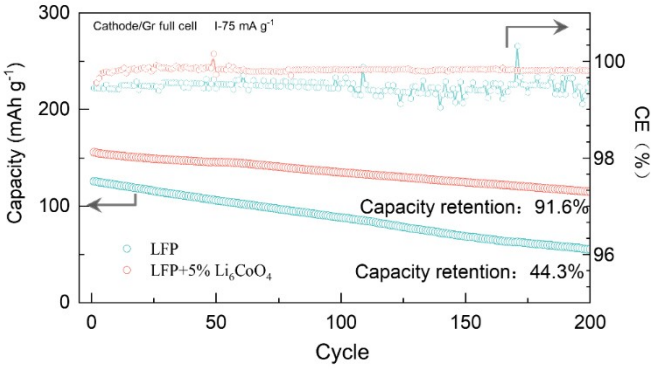

Supplementary Fig. 36| The cycle performance and coulombic efficiency of full cells with LFP and LFP+5% R-Li_6CoO_4 positive electrodes.

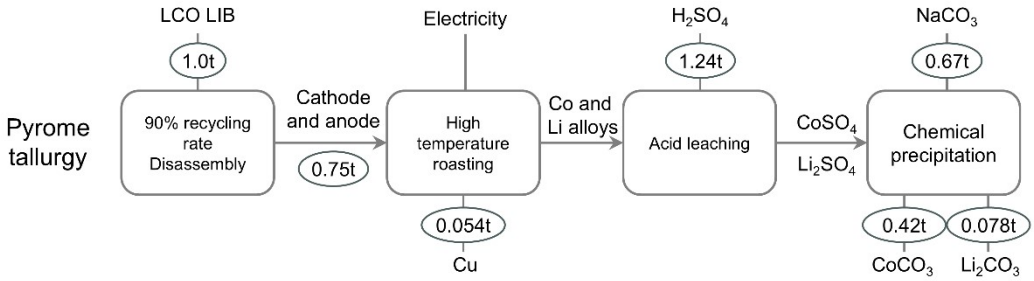

Supplementary Fig. 37| Material flow analysis of the pyrometallurgical recycling process. (Unit t: ton)

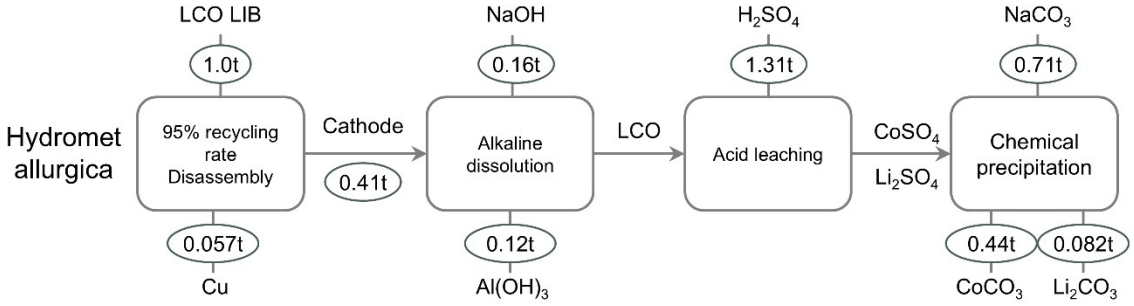

Supplementary Fig. 38| Material flow analysis of the hydrometallurgical recycling process. (Unit t: ton)

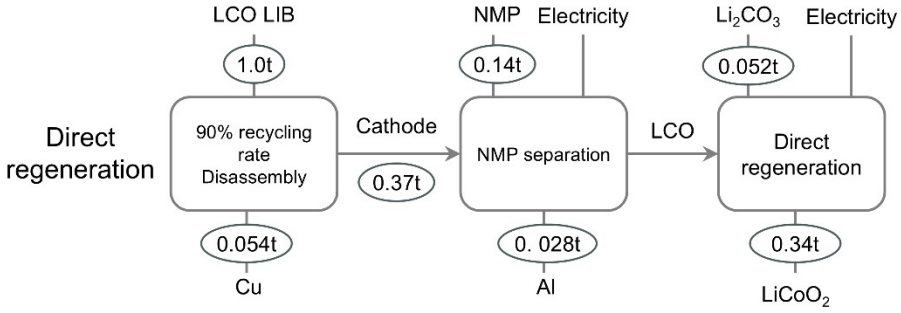

Supplementary Fig. 39| Material flow analysis of the direct recycling process. (Unit t: ton)

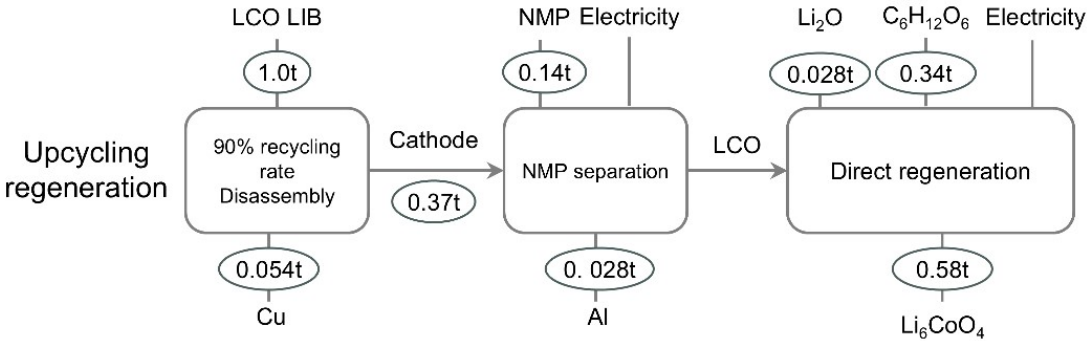

Supplementary Fig. 40| Material flow analysis of the up-recycling process in this work. (Unit t: ton)

Supplementary Tables

Supplementary Table 1| The atom ratios of lithium to cobalt in different samples.

Samples	Atom Ratio	
	Li	Co
S-LCO	0.732	1.00
Products of s-LCO and C after sintering with 550℃	0.715	1.00

Supplementary Table 2| Relevant parameters for Gibbs free energy calculations in Fig. 2b.

□	$LiCoO_2$	Li_2O	CoO	O_2				CO_2		
T1(K)	298.00	298.15	298.15	100.00	298.15	700.00	1200.00	50.00	298.15	900.00
T2 (K)	2500.00	1726.00	2078.00	298.15	700.00	1200.00	2500.00	298.15	900.00	2700.00
Phase	s	s	s	g	g	g	g	g	g	g
H (kcal/mol)	-162.38	-142.90	-56.87	0.00	0.00	0.00	0.00	-94.05	0.00	0.00
S (cal/(mol*K))	12.54	8.99	12.66	49.03	0.00	0.00	0.00	51.09	0.00	0.00
A (cal/(mol*K))	9.26	18.32	12.27	7.12	5.27	7.12	8.33	5.31	7.01	13.01
B	42.75	-3.26	0.07	-1.48	4.99	1.89	0.31	13.43	9.55	1.22
C	-1.94	-4.45	0.67	-0.01	0.39	-1.48	-3.38	0.03	-0.59	-10.42
D	-32.33	6.59	1.04	3.82	-1.96	-0.53	0.04	-5.38	-3.53	-0.19

Supplementary Table 3| The capacity utilization of R-Li_6CoO_4 in LFP+5% R-Li_6CoO_4 composites.

Item	Unit	Data
Mass of electrode	mg	3.25
Mass of LFP active materials	mg	2.7625
Mass of Li_6CoO_4 materials	mg	0.1625
Electrode capacity	mAh	0.5759
LFP contribution capacity	mAh	0.4537
Li_6CoO_4 contribution capacity	mAh	0.1222
Contribution of Li_6CoO_4 to specific capacity	mAh g^{-1}	752

Supplementary Table 4| The cost calculation per Ah for different prelithiation agents

	R-Li_6CoO_4		Li_5FeO_4		Li_2NiO_2	
Raw material	Li_2O	s-LCO	Li_2O	Fe_2O_3	Li_2O	NiO
1kg required raw material cost ($)	16.2	0.6	16.0	0.6	9.5	12.3
Raw material cost ($ kg^{-1})	16.8		16.6		21.8	
Specific Capacity (Ah kg^{-1})-Practical	860.0		588.0		400.0	
Cost ($ Ah^{-1})-Practical	0.020		0.028		0.054	
Li utilization rate	0.880		0.678		0.780	

Supplementary Table 5| The price of different materials involved in Table 4.

Material	Price ($ kg^{-1})	Source
Li_2O	33.1	https://dianchizhijia.com/
NiO	17.241	www.chemicalbook.com
Fe_2O_3	1.152	www.cbcie.com
Degraded LCO	5.366	https://dianchizhijia.com/

Supplementary Table 6| Design parameters of the battery cell.

Components	Item	Unit	Date
Cathode0	Active materials mass composition	/	96.5%
	Carbon black mass composition	/	1.50%
	Binder mass composition (PVDF)	/	2%
	LFP specific capacity	mAh g^{-1}	140
	LFP+5%Li6CoO4 specific capacity	mAh g^{-1}	165
	Coating surface density	g/m^2	205
	Positive current collector foil density (Al)	g/m^2	32
	Positive current collector foil thickness (Al)	mm	0.012
	Tab density (volume-averaged density) of positive	g/cc	2.6
	electrode materials positive electrode length	mm	30570

	electrode materials positive electrode width	mm	189
Anode	Active materials mass composition (graphite)	/	96%
	Carbon black mass composition	/	1
	Binder mass composition (CMC)	/	1.5%
	Binder mass composition (SBR)	/	2%
	Specific capacity (Graphite)	mAh g^{-1}	345
	Coating surface density	g/m^2	96.67
	NP ratio		1.15
	Negative current collector foil density (Cu)	g/m^2	54
	Negative current collector foil thickness (Cu)	mm	7
	Tab density (volume-averaged density) of Negative	g/cc	1.5
	electrode materials Negative electrode length	mm	30770
	electrode materials Negative electrode width	mm	193
	Neg electrode length	mm	308
	Neg electrode Width	mm	104
Electrolyte	Electrolyte weight	g	1100
Separator	Separator density	g/m^2	9.8
	Separator thickness	mm	0.012
	Separator porosity	/	50%
	Separator length	mm	31290
	Separator width	mm	197
Shell	Shell thickness	mm	0.4
	Shell length	mm	207
	Shell width	mm	173
	Shell height	mm	71
	Shell weight (Including the top cover)	g	365

Supplementary Table 7| Cost calculation of different recycling methods.

	Material cost	Disassembly cost	Electricity cost	Environmental governance cost	Direct labor	Depreciation
	Unit: $ t^{-1}					
This work	13895.2	143.0	99.4	100.3	223.8	57.0
Direct	4844.7	143.0	127.9	100.3	223.8	57.0
Hydro	4304.5	128.1	71.0	11.1	286.0	55.7
Pyro	4283.5	12.1	142.1	141.1	307.4	52.0

Supplementary Table 8| Income calculation of different recycling methods.

	Cu income	Al income	LCO income	All income
	Unit: $ t^{-1}			
This work	576.5	80.0	35811.7	36468.2
Direct	576.5	80.0	6531.2	7187.6
Hydro	608.5	4.8	5106.4	5719.7
Pyro	576.5	/	4837.7	5414.1

Supplementary Table 9| Profit calculation of different recycling methods.

	Profits
	Unit: $ t^{-1}
This work	21949.5
Direct	1691.0
Hydro	863.2
Pyro	476.0

Supplementary Table 10| The price of different materials involved in the above analysis.

Material	Price ($ t^{-1})	Source
Li_2CO_3	10,448	https://dianchizhijia.com/
$CoCO_3$	9,655	www.cbcie.com
AI	2,841	https://dianchizhijia.com/

Cu	10,675	https://dianchizhijia.com/
$LiCoO_2$	19,034	https://dianchizhijia.com/
H_2SO_4	64	www.100ppi.com
Na_2CO_3	234	www.chemicalbook.com
Electricity	0.14	
water	0.50	
Degraded LCO battery	29450	https://dianchizhijia.com/
NaOH	400	www.cbcie.com
Al $(OH)_3$	300	www.cbcie.com
NMP	12500	www.cbcie.com
Li_2O	33,103	www.cbcie.com
Li_5FeO_4	62,068	www.cbcie.com
Li_6CoO_4	62,068	Li_6CoO_4 price is consistent with the commercial price of Li_5FeO_4.
Glucose	413	www.100ppi.com

All specific prices and exchange rates are real-time prices of Feb 17, 2025, with the USD-CNY exchange rate of 7.25.